Journal of Power Sources 183 (2008) 693–700

Contents lists available at ScienceDirect

Journal of Power Sources

journal homepage: www.elsevier.com/locate/jpowsour

Enhanced hydrogen absorption kinetics for hydrogen storage using Mg flakes as compared to conventional spherical powders

Ki-Joon Jeon[a,1], Alexandros Theodore[b], Chang-Yu Wu[a,*]

[a] Department of Environmental Engineering Sciences, University of Florida, Gainesville, FL 32611-6450, USA
[b] Department of Chemical Engineering, University of Florida, Gainesville, FL 32611-6005, USA

ARTICLE INFO

Article history:
Received 12 March 2008
Received in revised form 7 May 2008
Accepted 8 May 2008
Available online 18 May 2008

Keywords:
Magnesium
Flake
Hydrogen storage
Dry coating
Nano-catalysts
Nickel
Kinetics

ABSTRACT

Practical challenges of metal hydrides for hydrogen storage such as magnesium hydride, lie predominantly in improving hydrogen absorption kinetics and capacity. Approaches to improving kinetics of Mg commonly include changing particle geometry, reducing crystallite size and coating with catalytic transition metals such as Ni. This study is aimed at improving the hydrogen storage kinetics and capacity of Mg by a novel approach utilizing high aspect ratio powders (thin metal flakes with large diameters) coated with a Ni nano-catalyst. A high speed orbiting ball media (HSOBM) processor was utilized to fabricate the flake-shaped materials. Mg flakes effectively coated with Ni nano-catalyst using dry mechanical coating were found to possess more favorable hydrogen absorption/desorption characteristics and improved hydrogen storage capacity than traditional spherical particles. Geometric shape was shown to be a vital factor in hydrogen absorption kinetics and its effects proved to be dominant over those of crystallite size.

1. Introduction

Among the various light metals and alloys that are capable of absorbing/desorbing large amounts of hydrogen, magnesium has been considered a promising candidate for solid hydrogen storage due to its high volumetric/gravimetric capacity, ease of availability and low cost [1,2]. The hydrogenation process starts from physisorption of hydrogen molecules onto the surface of magnesium particles, followed by dissociation into hydrogen atoms. The hydrogen atoms thus obtained diffuse into magnesium lattices to initiate nucleation and growth of magnesium hydride [3–5]. However, the major disadvantage of utilizing pure magnesium is its slow absorption of hydrogen, which is due to its low affinity for hydrogen physisorption, and the formation of a dense magnesium hydride layer [1,4,6]. The hydride layer becomes a resistive barrier for subsequent hydrogen diffusion into the bulk and therefore results in limited material utilization. This ultimately becomes a crucial rate-limiting mechanism in the hydrogenation process [5,7,8].

Various attempts have been undertaken to chemically improve the kinetics of Mg by incorporating transition metals such as Ni, V, Fe and Ti [8–15]. The addition of transition metals with high affinities for chemisorption results in interfacial catalysis of H_2 dissociation thus reducing the activation energy required for dissociation of hydrogen molecules [16,17]. The resultant hydrogen atoms can more easily diffuse along grain boundaries of magnesium than H_2 [18,19]. Consequentially, it has been demonstrated that the onset temperature for hydrogen absorption can be lowered by approximately 170 °C by adding a small amount of Ni onto Mg [9]. Studies report that a homogeneous distribution of nano-catalysts on the metal drastically reduces the activation energy of hydrogen diffusion and results in faster formation of metal hydride even in the presence of oxides and hydroxides [20–23]. However, it should be noted that when hydrogen diffusion was the rate-limiting mechanism, excessive Ni wt.% loading showed negligible impact on H_2 absorption rate and capacity [8]. In addition, the particle diameter of the catalyst has been also recognized as an influential parameter. Varin et al. [15] investigated the effect of Ni particle size (micro, submicron and nano-sizes) on the hydrogen absorption/desorption kinetics of 44 μm Mg powder. The addition of nano-Ni was observed to greatly improve the hydrogen absorption/desorption rate as compared to micron/submicron sized catalysts.

The kinetics of hydrogen absorption and desorption of metal hydrides have also been improved mechanically by increasing the specific surface area and number of grain boundaries, reducing the crystallite size, and altogether enhancing diffusion of hydrogen

* Corresponding author. Tel.: +1 352 392 0845; fax: +1 352 392 3076.
E-mail address: cywu@ufl.edu (C.-Y. Wu).
[1] Present address: Environmental Energy Technologies Division, Lawrence Berkeley National Laboratory, Berkeley, CA 94720, USA.

0378-7753/$ – see front matter © 2008 Elsevier B.V. All rights reserved.
doi:10.1016/j.jpowsour.2008.05.033

Nomenclature

d_m	diameter of Mg (m)
d_n	diameter of Ni (m)
h	initial thickness of Mg flakes (m)
P	hydrogen pressure (Pa)
V	volume of chamber (m^3)
R	ideal gas constant (m^3 Pa K^{-1} mol^{-1})
T	temperature (K)
X_{sph}	minimum wt.% of catalyst for spherical particle (wt.%)
X_{fla}	minimum wt.% of catalyst for flake particle (wt.%)

Greek letters

α	metal hydride volume fraction
ρ_m	molar density of Mg particle (mole m^{-3})
ρ_n	molar density of Ni particle (mole m^{-3})
Ψ	critical hydrogenation capacity

atoms within the metal bulk leading to increased hydride formation [9–13,15,24–28]. Most past research studies such as these have been conducted based on magnesium particles processed by conventional ball milling due to their ability to change the microstructure of the magnesium.

A better understanding of the overall process of hydrogenation is needed to further develop the practicality of magnesium as a storage option. In the beginning of the process, nucleation of MgH_2 is the rate-liming mechanism; however, hydrogen diffusion through the impermeable hydride layer eventually becomes the rate-liming mechanism once the hydride layer reaches a critical thickness. The maximum penetration depth for nucleation-limited condition for a 44 μm sample was calculated to be 6 μm [8]. Since a short fuelling time is critical to practical applications, it is advantageous to accomplish the majority of hydrogen uptake while it is in the most rapid nucleation-limited stage. In order to reduce the limiting effect of diffusion through the compact MgH_2 layer and thereby extend the nucleation-limited stage, particles with high specific surface area are favored. This is because they increase the number of surface reaction sites and decrease the necessary diffusion depth required to utilize the entire bulk volume. Nano-sized Mg particles and thin Mg films have been used to minimize this problem; however, practical production costs of these materials may be a concern.

The effect of geometry on the hydrogen absorption kinetics of magnesium particles has not yet been explored in depth. Developments of new material production technologies that improve material utilization and increase production efficiency are very much sought after. Recently, a high speed orbiting ball media (HSOBM) processor was successfully introduced as a fast and efficient method to fabricate flake-shaped magnesium particles with high specific surface areas [29], although its impact on hydrogen uptake has not been evaluated yet.

The objective of this study was to maximize the nucleation-limited regime, to improve material utilization and to enhance hydrogen uptake by changing either geometry or crystallite size of Mg. Spherical and flake-shaped particles were characterized by crystallite size and hydrogenation characteristics. The HSOBM processor was also tested for its ability to coat the nano-catalyst on magnesium flakes in order to evaluate its potential for combined flake/coating processor. The coating efficiency of both the HSOBM processor and a dry mechanical coating processor (Theta Composer) were assessed. Finally, the effects of geometry on hydrogen absorption kinetics were analyzed from hydrogenation data.

2. Experimental methodology

2.1. Fabrication of Mg flake–nano-Ni composites

Mg flakes were prepared using a HSOBM processor. The coating of nano-Ni catalysts was carried out using either a HSOBM processor or a Theta Composer (Tokuju, Corp.) under an argon environment. In-depth details of the mechanistic aspects of the processes have been described elsewhere [8,29,30], and only a brief description is provided here.

The Theta Composer consists of an elliptic rotor encased in a vessel. The rotor operates at high revolution while the vessel counter-rotates at a lower speed. During rotation it applies strong compression and shear forces to the particles as they pass through the narrow gap between the rotor and vessel wall [8,30,31]. The process also more evenly distributes the Ni nanoparticles onto the magnesium surface. The rotor and vessel are made of stainless steel in order to maintain an inert environment and prevent chemical reactions. The HSOBM processor uses ball media rolling on the walls inside a tube at high speeds to create strong compression and shear forces, flattening particles as they pass between the rolling media and the vessel wall. In a likewise manner, the high speeds and large compression and shear forces are capable of breaking up nano-agglomerates and coating the nanoparticles on the Mg flake.

The basic procedure used in creating Mg–Ni flake composites is as follows: 25 mg magnesium (Fisher Scientific, 294 μm) and 6.0 mm balls (Chromium-Steel Cr-52100, Norstone Inc.) were introduced into the HSOBM tube in a glove box (oxygen level was lower than 0.5 ppm). The milling system was operated with an orbiting speed of 13,000 rpm, and with 2-min milling time. After each milling process, 3 wt.% of the nano-Ni (primary particle size: 72 ± 30 nm, surface area: 6 m^2 g^{-1}, bulk density: 0.66 g cm^{-3}, Argonide) was added to the Mg flakes. The mixture was then either coated for 2 min with ball speeds of 13,000 rpm in the HSOBM with 2.0 mm ball sizes, or for 90 min with the Theta Composer running at 4600×70 rpm.

The surface area analysis was performed on a Quanta Chrome NOVA 1200 Gas Sorption Analyzer using a N_2 adsorption isotherm with a multi-point Brunauer–Emmett–Teller (BET) method. Scanning Electron Microscopy (SEM, JEOL JSM 6335F) coupled with Energy Dispersive Spectroscopy (EDS) was used for comparing surface morphologies on the magnesium powders before and after milling process and dispersion of nano-catalysts on the surface of Mg flake. To determine the thickness of the flake particles, they were suspended and solidified in an epoxy resin. The dried epoxy was then polished to obtain cross sectional slices of flakes and subsequently examined under an optical microscope (Olympus BX-60). The formation of MgH_2 in the Mg–Ni flake composites, the orientation of crystal structure and the crystallite refinements and lattice strains of flakes were determined by X-ray diffraction (Phillips XRD APD 3720) with a 2θ range of 20–70° with 3 s of count time per step.

2.2. H_2 absorption/desorption characterization

Hydrogen absorption experiments were carried out in a hydrogenation system. The hydrogenation system is shown in Fig. 1. 0.905 g of the Mg–Ni flake composite was introduced into the hydrogenation chamber while in a glove box. After the chamber was installed in the system, it was flushed three times with argon to eliminate possible contamination. In vacuum, the hydrogenation chamber was heated to the target temperature (483 K). Pure grade hydrogen (4.8) was then instantly introduced into the hydrogenation chamber at 1 MPa and hydrogen pressure was maintained constant by means of a regulator between a high-pressure reservoir (initial pressure of 2.41 MPa) and the chamber. The temperature

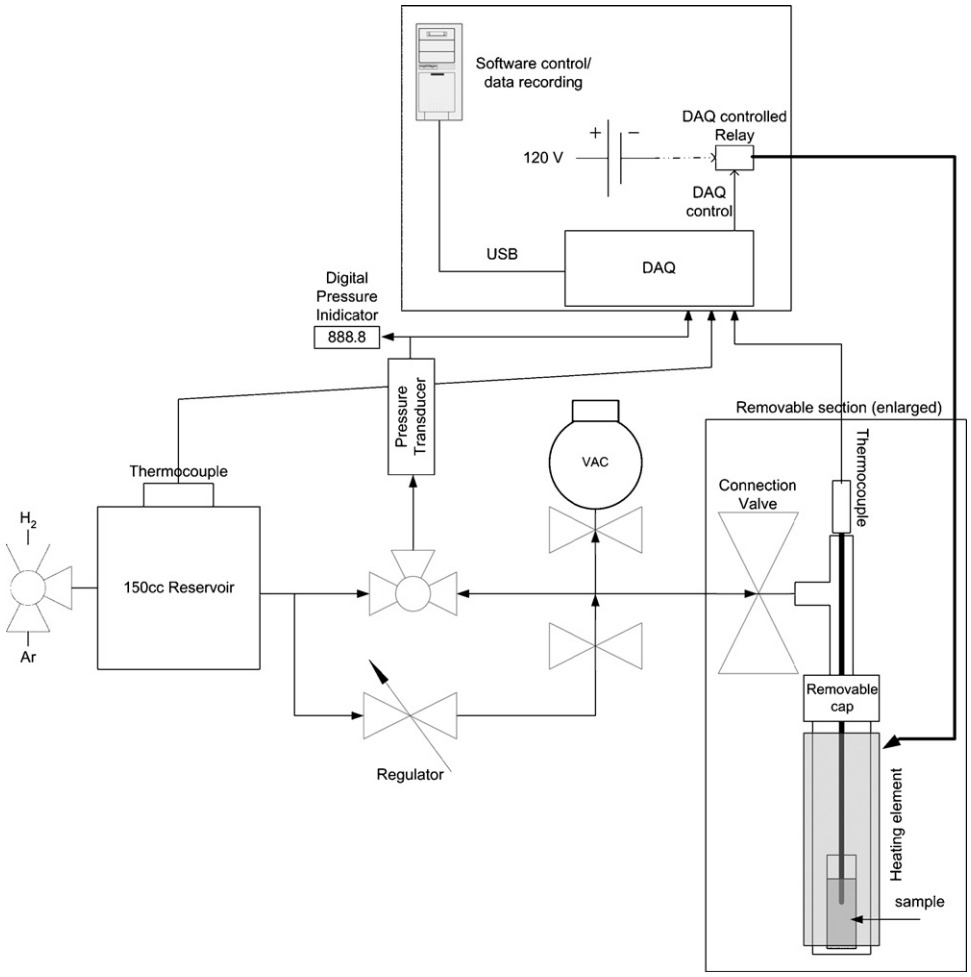

Fig. 1. Schematic diagram of hydrogenation system.

Table 1
Experimental conditions

Sample	Particle size and shape	Ni (wt.%)	Milling time (min)	Coating time (min)	Predicted (wt.%)	TGA (wt.%)
1	44 μm Mg sphere	2	0	90[a]	4.19	4.2
2	294 ± 155 μm Mg sphere	0	0	0	0.00	–
3	442 ± 386 μm Mg flakes	0	2	0	0.01	–
4	438 ± 328 μm Mg flakes	3	2	2[b]	3.31	3.32
5	427 ± 293 μm Mg flakes	3	2	90[a]	4.62	4.57

[a] Coating method: Theta Composer.
[b] Coating method: HSOBM.

of the chamber was monitored by a thermocouple (Fisher Scientific model 15-078-39, type K) and the hydrogen pressure in the reservoir was monitored using an electronic pressure transmitter (Omega, PX880).

After the hydrogenation process, the Mg–Ni flake composites were analyzed by a Thermo Gravimetric Analyzer (TGA) to determine the amount of hydrogen absorbed in the Mg–Ni flake composites. A *PV*/*RT* value in unit of mole was utilized to associate pressure and temperature effects simultaneously and used to compare experimental data to theoretical prediction. $\Delta PV/RT$ data, calculated from the measured pressure loss in the 150 cm^3 reservoir, were accurate to within 1.5% of the experimental data from TGA [8], and was used in subsequent analyses in this study. Although there are many parameters that affect hydrogen absorption/desorption rate, two of the more important ones, namely change in particle geometry and Ni loading, were evaluated while other conditions were kept constant in this study. The experimental conditions are listed in Table 1.

3. Results and discussion

3.1. Determination of minimum Ni loading

Prior to experimentation, the minimum nano-Ni loading for spherical and flake-shaped particles was theoretically investigated. A minimum nano-Ni wt.% is defined as the Ni wt.% required to form monolayer coverage on the surface of Mg powder. For spherical/flake particles, the minimum Ni loading can be expressed by Eqs. (1) and (2) respectively:

$$X_{\mathrm{sph}} = \frac{1}{(1/\pi)(d_{\mathrm{m}}/d_{\mathrm{n}})(\rho_{\mathrm{m}}/\rho_{\mathrm{n}}) + 1} \quad (1)$$

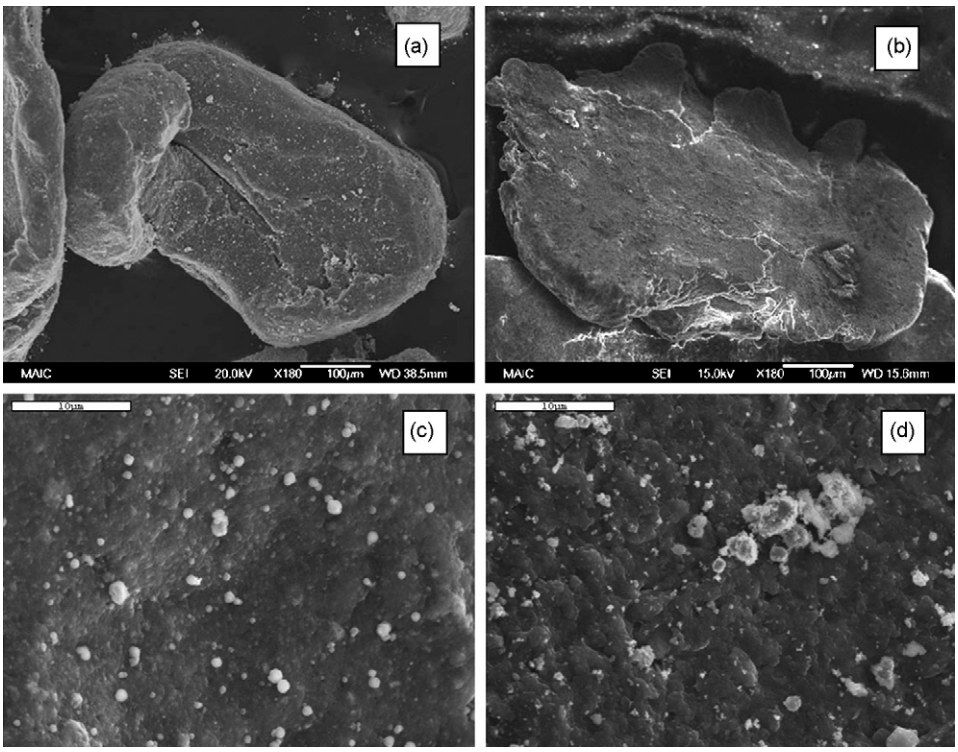

Fig. 2. Surface morphology change: (a) sample 2 (pure 294 μm Mg, 180×); (b) sample 3 (Mg flakes, 180×); (c) sample 5 after Theta Composer (294 μm Mg flake–Ni composites, 2000×); (4) sample 4 (Mg flake–Ni composites, 2000×).

$$X_{\mathrm{fla}} = \frac{1}{(3/\pi)(d_{\mathrm{m}}h/(d_{\mathrm{n}}(d_{\mathrm{m}}+2h)))(\rho_{\mathrm{m}}/\rho_{\mathrm{n}})+1} \quad (2)$$

The average thickness and diameter of flakes, measured to be 11.73 μm and 442 μm respectively under optical microscopy (Olympus BX-60), were used in this calculation [29]. For 70 nm Ni, X_{fla} was found to be 3.14 wt.% for flakes while X_{sph} was calculated to be 2.1 wt.% for the 44 μm Mg. Thus, Ni loading in excess of 3 wt.% was not considered. Furthermore, loss in hydrogen capacity resulting from a heavier weight could render the material less practical for onboard storage [2,12,32].

3.2. Characterization of Mg flakes (SEM/BET/XRD)

Geometric examination of the magnesium powders before and after the HSOBM process was conducted using SEM. By comparing the images of pure 294 μm spherical Mg and Mg flakes in Fig. 2(a) and (b), it was observed that after milling with HSOBM, Mg showed observable physical surface changes and reduction in thickness. The specific surface area of the powders before and after processing in the HSOBM was also measured using BET; however, the surface area was of too low magnitude (<0.5 $m^2\ g^{-1}$) to have reliable results.

The XRD spectra of the structural evolution of pure Mg are shown in Fig. 3(b) and (c). After 2 min milling with HSOBM, the 1st highest peak (36.6°) for pure Mg is significantly reduced in intensity. On the other hand, the intensity of the 2nd highest peak for pure Mg reaches a significant peak after 2 min milling using the HSOBM processor. It was noted that the orientation of crystal structure of Mg, shown in Fig. 3, was changed from 36.6° to 34.5°. This could be due to plastic deformation shear/compression forces experienced by Mg during the HSOBM milling process [29,33] which would result in a change in the orientation of crystal structure, crystallite refinement of Mg flakes and change of lattice strains. The crystallite refinements and lattice strains of Mg flakes for 34.5° (orientation: 0 0 0 2) peaks were also determined by single line profile analysis in addition to XRD [36]. It was observed that the average crystallite size of flakes (316.3 nm with 0.26% lattice strain) becomes smaller than those of 294 μm Mg powder (423.4 nm with 0.19% lattice strains) within 2 min of processing time. The average crystallite size of 44 μm Mg powder is 132.3 nm with 0.16% lattice strain. It should be noted that instrumental broadening was not accounted for and therefore care should be exercised in using the values for quantitative comparison.

The crystalline phase of Mg and Ni was preserved during processing and coating by HSOBM and Theta Composer, and no XRD peaks of Mg_xNi_y alloy were observed, as shown in Fig. 3(a), (d), and (e). After hydrogenation, the formation of MgH_2 was observed in samples 1, 4, and 5.

3.3. Effect of crystallite size on H_2 absorption kinetics without nano-catalyst

Several studies [22,34,35,37] have reported that the reduction of crystallite size increases the number of paths for hydrogen diffusion as well as nucleation sites for reaction, which altogether enhances hydrogen absorption kinetics. Past studies have shown that particles with nano-sized grains, which have been mechanically milled for long periods (greater than 300 h), have been known to have appreciable hydrogen absorption without the need for catalysts while also reacting at relatively low temperatures [35,37]. To investigate the effects of average crystallite size of Mg powder before and after milling on hydrogen absorption capacity, 294 μm spherical Mg powders were milled for 2 min to form 442 μm flakes (with 11.7 μm thickness), i.e. samples 1 and 2, respectively. Hydrogenation tests were performed for these samples that had no Ni catalysts coating. Fig. 4 shows the effects of crystallite size on the hydrogen absorption capacity. Although the thin flake-shaped particle with smaller crystallite size was used, as shown, there was no evidence of hydrogen absorption in either of the pure Mg sam-

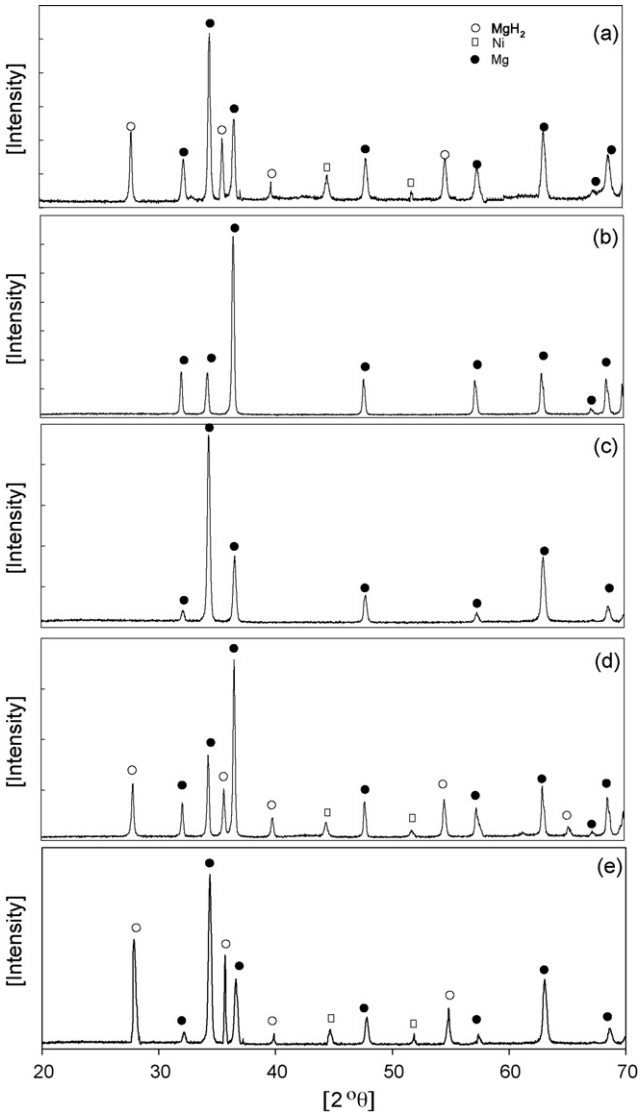

Fig. 3. Comparison of XRD patterns: (a) sample 4 after hydrogenation; (b) sample 2 before HSOBM processing; (c) sample 3 after 2 min HSOBM processing; (d) sample 1 after hydrogenation; (e) sample 5 after hydrogenation.

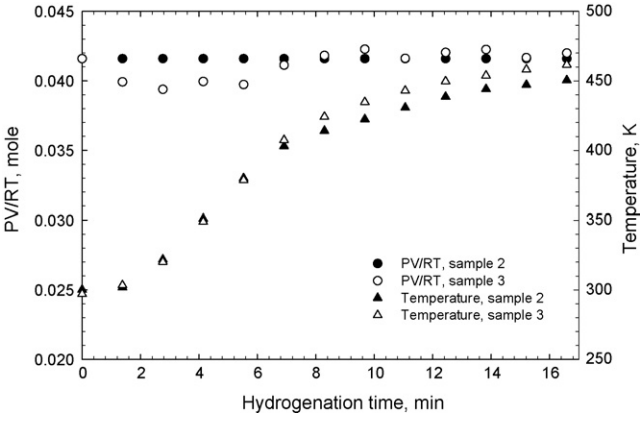

Fig. 4. Effect of morphological change without catalysts on hydrogenation.

ples. Therefore, it can be inferred that in the absence of Ni catalysts the reduction of crystallite size produced by the HSOBM processor has negligible effect on hydrogen absorption capacity. This confirms the precedence of the Ni catalyst for feasible hydrogen absorption in Mg particles. It also shows a deviation from previous studies, which indicated that powders with reduced crystallite sizes hydrogenated without the aid of nano-catalysts [35,37]. The most likely reason for this deviation is that the flake samples did not have a sufficiently small crystallite size (100 nm) because of the short milling time that was constrained by the mechanical limitations of the device.

3.4. Analysis of coating methods and change of thickness

The effective dispersion of catalysts and geometry change were also investigated with two methods (HSOBM and Theta Composer). Fig. 5 shows a homogeneous distribution of nano-Ni on the Mg powder/flake surface under SEM-EDS. The dispersion of nano-Ni was further assessed quantitatively using Spot Advanced (Diagnostic Instrument, Inc.) image capture software [29,30,38]. Thirty equally divided areas were randomly selected from the EDS images of Ni on the Mg substrate. The number of individual Ni clusters was determined in each area and statistical analyses were performed. It is observed from Fig. 6 that 2 min coating with HSOBM yielded Ni clusters that were larger in size but fewer in number with a lower mean (number of clusters) and standard deviation (23.7 and 5.59, respectively) as compared to that of Theta Composer with 90 min coating time (50.76 and 8.76, respectively). Fig. 6 also shows that 44 μm Mg coated with Theta Composer yielded Ni clusters with a similar mean (number of clusters) and standard deviation (55.4 and 8.10, respectively) as compared to Mg flakes with the Theta Composer (50.76 and 8.76, respectively). This comparative analysis confirmed that Ni nanoparticle dispersion was more effective with Theta Composer. This is mostly a result of the short operating times of the HSOBM device (due to mechanical limitations of the lab-scale process) but may also be a result of its high coating speeds, which have been known to subdue coating efficiency due to a nano-lubrication effect [39,40].

Thickness change was measured after Theta Composer and HSOBM coating under optical microscope (Olympus BX-60). The average thickness of flakes (samples 3 and 4) was 11.73 μm and 11.76 μm, respectively, after coating with HSOBM. After Theta Composer coating the average thickness of flakes (sample 5) increased from 11.73 μm to 16.87 μm.

3.5. Effect of nano-catalysts dispersion on H_2 absorption kinetics

Fig. 7(a) plots the hydrogen absorption data for samples 1, 4 and 5, as a function of time. It can be seen that the least effective of these was sample 4, which was a flake particle using the HSOBM coating method. These poor results are most likely due to insufficient catalytic enhancement and are supported by the low coating quality reported in Section 3.4. Samples 1 and 5 were coated using the more efficient Theta Composer and showed significant hydrogen absorption capacities of 4.19 wt.% and 4.62 wt.% respectively, after 300 min. The hydrogen absorption capacities for samples 1, 4 and 5 were also confirmed using TGA analysis and can be seen in Fig. 7(b). This analysis supports the trend that hydrogen absorption capacity is largely dependant on an effective Ni catalyst coating. In order to appreciate the effect of surface area for each sample's results, the specific surface area of each sample was estimated assuming spherical particles or smooth flakes of uniform thickness and diameter. The results gave that samples 4 and 5 shared relatively close specific surface areas to sample 1, with ratios of 1.31:1 and 0.931:1. It can therefore be reasonably inferred that difference in surface area had negligible impact on the observed trends.

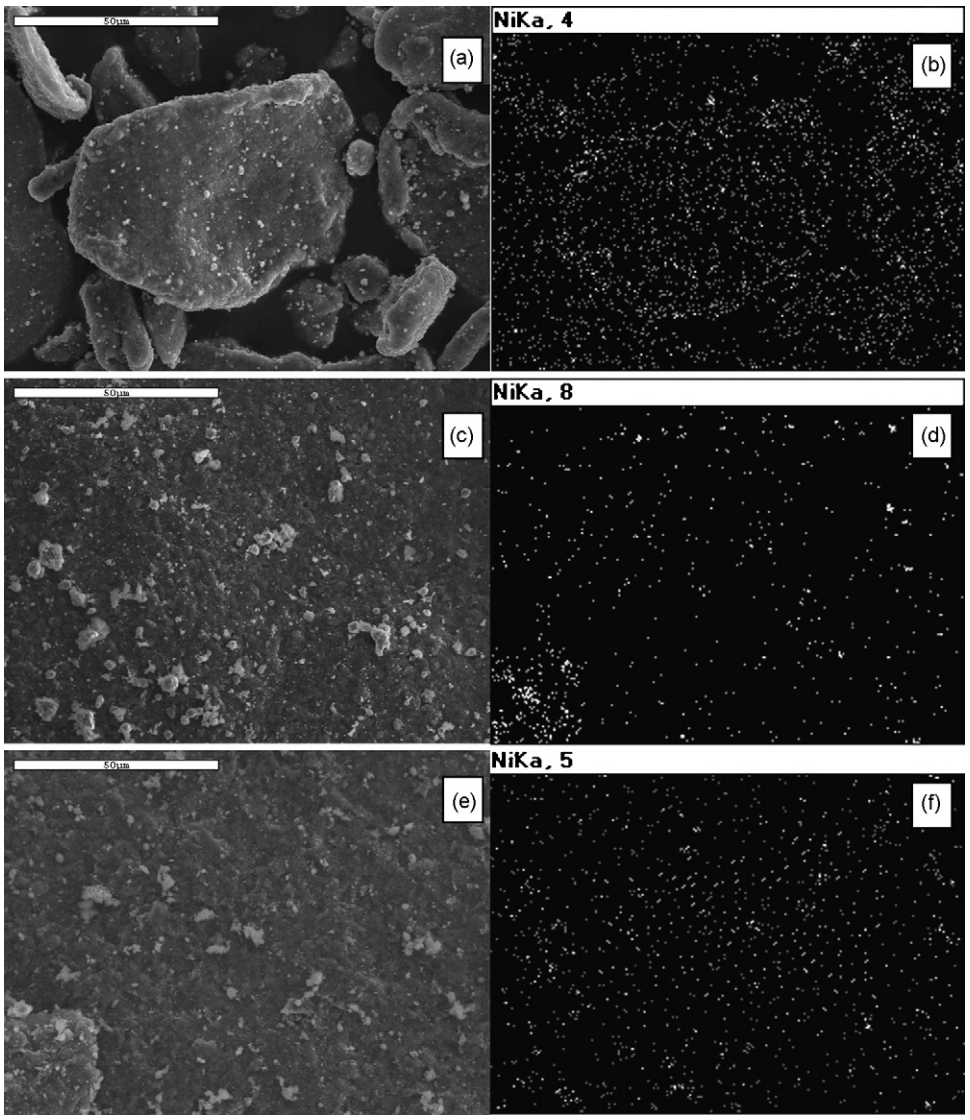

Fig. 5. Distribution of Ni nanoparticles on Mg (a) SEM image (sample 1); (b) Ni mapping (sample 1); (c) SEM image (sample 4); (d) Ni mapping (sample 4); (e) SEM image (sample 5); (f) Ni mapping (sample 5). Scale bars are all 50 μm.

3.6. *Effect of geometric change on H_2 absorption kinetics*

To closely observe the effect of coating efficiency and particle geometry on kinetics, a hydrogen absorption rate vs. metal hydride volume fraction (α) [8] plot was rendered in Fig. 8. The initial observations support earlier conclusions that sample 5 shows the highest initial absorption rate followed by sample 1, with the least absorption rate by sample 4. When α is approximately 0.28, the rate of absorption for well-coated flakes was approximately four times that of poorly coated flakes. Coating efficiency can therefore be seen to drastically affect the kinetics when comparing flakes-shaped particles.

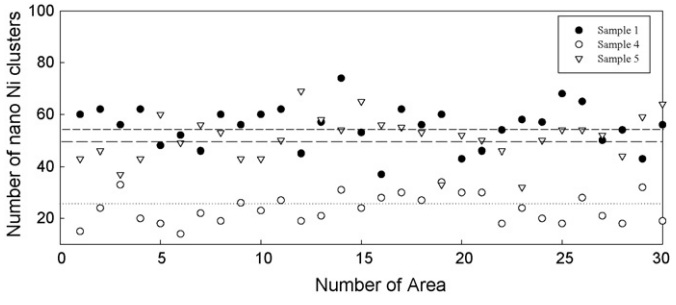

Fig. 6. Nano-Ni uniformity measurements on the Mg flakes fabricated by HSOBM and Theta Composer.

The effect of particle geometry on kinetics can also be observed between samples of spherical and flake particles which were both effectively coated with Ni catalyst using the same methodology. Compared to sample 1 of spherical particles, sample 5 clearly shows a shift towards higher reaction rates and capacities. This shift of the sample regression lines towards higher hydrogen absorption represents an increase in the critical hydrogenation capacity (Ψ). Ψ is the point at which the hydrogen absorption kinetics have a very evident change in rate. This is interpreted as the point switching from the nucleation-limited (faster) to diffusion-limited (slower) regime [8] and is qualitatively shown on Fig. 8 as the approximate intersection of the curve's tangential lines. Comparing samples 1 and 5, the larger value of Ψ_5 implies that the change in geometry from spherical to flake-shaped particle produces a prolonged nucleation-limited period. This ultimately leads to a higher absorp-

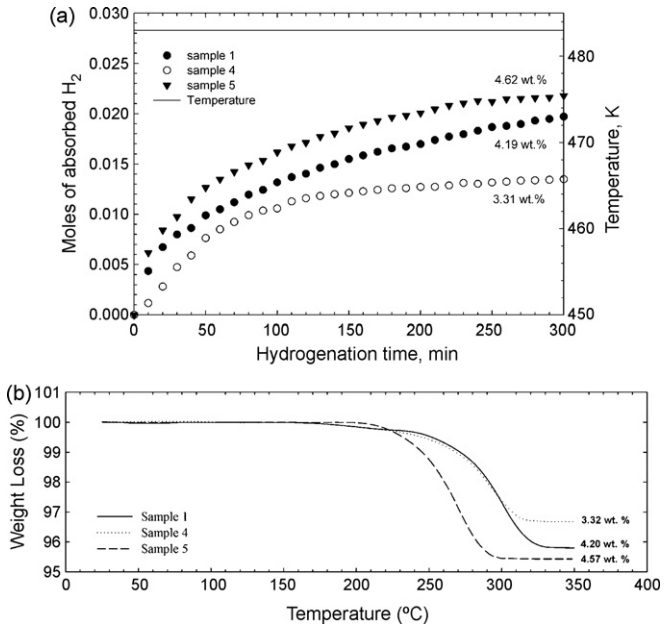

Fig. 7. Effect of dispersion of nano-catalyst on: (a) hydrogen absorption ($\Delta PV/RT$); (b) hydrogen desorption analysis by TGA.

tion capacity in a given period of time for flake-shaped particles, as observed in Fig. 7. This analysis also supports the poor results of sample 4, as its regression line is shifted towards lower hydrogen absorption area in Fig. 8. This is known already to be a result of poor coating efficiency, which is evident when compared with sample 5 of the same geometry. The observed effects of particle geometry on hydrogen absorption can be reasonably understood based on a simple macroscopic comparison of hydrogen diffusion under rectangular (flake particles) vs. radial (spherical particles) coordinates. For rectangular coordinate systems, as hydrogen diffuses into the Mg flake, the flux area remains relatively constant with respect to the hydrogen penetration depth. However, for spherical particles understood through a radial coordinate system, as the hydrogenation layer thickens, the available flux area reduces with decreasing radius. This results in a diffusion term that reduces as a function of time and subsequently brings upon a diffusion-limited case earlier than in the rectangular coordinate system. It should be pointed out that although these data give us valid trends, the initial values of α have very high reaction rates that were beyond the detection resolution of our equipment. Therefore, these values (Ψ) are roughly estimated, and more sophisticated equipment is needed for accurate measurement in that regime.

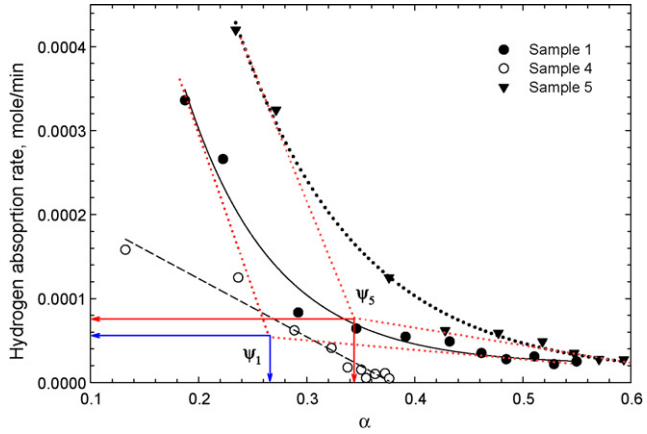

Fig. 8. Effects of particle geometry and coating efficiency on the hydrogen absorption kinetics (0.905 g for each sample).

Previous research has emphasized that reduced crystallite size of the particle is also an important factor in hydrogenation [22,34,35]. For sample 1, the crystallite size of the 44 μm powder was significantly smaller than that of the flakes in sample 5, implying that the hydrogen absorption capacity and rate of absorption should be much better than that of the flakes. Since this was not the result in this study, it is therefore inferred that the effect of geometry on hydrogen capacity and absorption rate is dominant over the effect of crystallite size in the ranges encountered. These results show that flake particles which had nearly equal coating efficiency and specific surface area as that of the spherical 44 μm sample exhibited improved absorption kinetics and capacities over spherical particles.

4. Conclusion

This study aimed at enhancing hydrogen uptake kinetics and storage efficiency by utilizing thin Mg flakes with large diameters coated with nano-Ni catalysts. XRD analyses of the product processed by the HSOBM process showed a change in the orientation of crystal structure of Mg, and a reduction in crystallite size; however, this change was not large enough to hydrogenate uncoated Mg flakes. The individual crystalline phase of Mg and Ni was preserved and no XRD peaks of Mg_xNi_y alloy were observed after processing with HSOBM or when coating with a Theta Composer. Comparisons between samples of flakes without Ni coating, and with coating by the HSOBM processor and Theta Composer confirmed the need of well-dispersed nano-catalyst particles for practical hydrogenation systems.

Hydrogenation absorption trends showed that flakes benefited from longer nucleation-limited periods than spherical particles, which lead to higher initial absorption rates and higher final absorption capacities. Geometry was identified to be a critical component affecting hydrogen absorption capacity and kinetics, and appeared to be a dominant contributor over the effects of crystallite boundary.

Acknowledgements

Ki-Joon Jeon is grateful to the University of Florida Alumni Fellowship and Korean Science & Engineering Foundation's Graduate Study Abroad Scholarship Program (M06-2003-000-10264-0). Alexandros Theodore is grateful to Dr. Dale Lundgren for the EPA Air Pollution Training Scholarship and to the Particle Engineering Research Center (PERC) at University of Florida for the Undergraduate Research Scholarship. We would like to acknowledge Major Analytical Instrument Center (MAIC) and PERC at University of Florida, for analytical instrumentation as well as Tokuju Corporation for providing Theta Composer. We also thank Dr. Wolfgang Sigmund at University of Florida for his TGA, Dr. Satoru Watano at Osaka Prefecture University for insightful knowledge of dry mechanical coating and Dr. Mei Cai at General Motors for in-depth knowledge in hydrogen research.

References

[1] L. Schlapbach, A. Zuttel, Nature 414 (6861) (2001) 353–358.
[2] S.G. Chalk, J.E. Miller, Journal of Power Sources 159 (1) (2006) 73–80.
[3] W.C. Conner, J.L. Falconer, Chemical Reviews 95 (3) (1995) 759–788.
[4] Y. Fukai, The Metal–Hydrogen System: Basic Bulk Properties, 2nd rev. and updated ed., Springer, Berlin, 2005, p. 497.
[5] J. Bloch, M.H. Mintz, Journal of Alloys and Compounds 253 (1997) 529–541.

[6] P.W. Atkins, J. DePaula, Physical Chemistry, 7th ed., W.H. Freeman, New York, 2002, p. 1139.
[7] G. Friedlmeier, M. Groll, Journal of Alloys and Compounds 253 (1997) 550–555.
[8] K.J. Jeon, A. Theodore, C.Y. Wu, M. Cai, International Journal of Hydrogen Energy 32 (11) (2007) 1860–1868.
[9] R.L. Holtz, M.A. Imam, Journal of Materials Science 34 (11) (1999) 2655–2663.
[10] G. Liang, S. Boily, J. Huot, A. Van Neste, R. Schulz, Journal of Alloys and Compounds 267 (1–2) (1998) 302–306.
[11] J. Huot, G. Liang, S. Boily, A. Van Neste, R. Schulz, Journal of Alloys and Compounds 295 (1999) 495–500.
[12] A. Zaluska, L. Zaluski, J.O. Strom-Olsen, Journal of Alloys and Compounds 288 (1–2) (1999) 217–225.
[13] C. Iwakura, H. Inoue, S. Nohara, R. Shin-ya, S. Kurosaka, K. Miyanohara, Journal of Alloys and Compounds 330 (2002) 636–639.
[14] C. Iwakura, S. Nohara, S.G. Zhang, H. Inoue, Journal of Alloys and Compounds 285 (1–2) (1999) 246–249.
[15] R.A. Varin, T. Czujko, C. Chiu, Z. Wronski, Journal of Alloys and Compounds 424 (1–2) (2006) 356–364.
[16] F. Stil Stillesjo, B. Hjorvarsson, B. Rodmacq, Journal of Magnetism and Magnetic Materials 126 (1–3) (1993) 102–104.
[17] G. Sandrock, K. Gross, G. Thomas, Journal of Alloys and Compounds 339 (1–2) (2002) 299–308.
[18] V.V. Rozanov, O.V. Krylov, Uspekhi Khimii 66 (2) (1997) 117–130.
[19] A.D. Lueking, R.T. Yang, Applied Catalysis A-General 265 (2) (2004) 259–268.
[20] M. Au, Materials Science and Engineering B-Solid State Materials for Advanced Technology 117 (1) (2005) 37–44.
[21] A.M. Seayad, D.M. Antonelli, Advanced Materials 16 (9–10) (2004) 765–777.
[22] A. Zaluska, L. Zaluski, J.O. Strom-Olsen, Applied Physics a-Materials Science & Processing 72 (2) (2001) 157–165.
[23] J. Huot, G. Liang, R. Schulz, Applied Physics a-Materials Science & Processing 72 (2) (2001) 187–195.
[24] Á. Révész, D. Fátay, T. Spassov, Journal of Alloys and Compounds 434–435 (2007) 725–728.
[25] J. Huot, E. Akiba, et al., Journal of Alloys and Compounds 231 (1) (1995) 815–819.
[26] S. Doppiu, V. Langlais, J. Sort, S. Surinach, M.D. Baro, Y. Zhang, G. Hadjipanayis, J. Nogues, Chemistry of Materials 16 (26) (2004) 5664–5669.
[27] P. Tessier, E. Akiba, Journal of Alloys and Compounds 295 (1999) 400–402.
[28] Z.X. Yu, Z.Y. Liu, E.D. Wang, Materials Science and Engineering a-Structural Materials Properties Microstructure and Processing 335 (1–2) (2002) 43–48.
[29] A. Theodore, K.J. Jeon, C.Y. Wu, KONA 24 (2006) 83–92.
[30] N. Coowanitwong, C.Y. Wu, M. Cai, M. Ruthkosky, J. Rogers, L. Feng, S. Watano, T. Yoshida, Journal of Nanoparticle Research 5 (3–4) (2003) 247–258.
[31] D. Cooper, C.Y. Wu, D. Yanskey, D. Butt, M. Cai, KONA (2005) 139–151.
[32] DOE, Hydrogen Posture Plan: An Integrated Research, Development and Demonstration Plan. 2007; http://www.hydrogen.energy.gov/news_posture.htm.
[33] W.D. Callister, Material Science and Engineering, Wiley, New York, 2002, p. 854.
[34] M. Dornheim, N. Eigen, G. Barkhordarian, T. Klassen, R. Bormann, Advanced Engineering Materials 8 (5) (2006) 377–385.
[35] M. Dornheim, S. Doppiu, G. Barkhordarian, U. Boesenberg, T. Klassen, O. Gutfleisch, R. Bormann, Scripta Materialia 56 (10) (2007) 841–846.
[36] B.D. Cullity, S.R. Stock, Elements of X-Ray Diffraction, Prentice Hall, New Jersey, 2001, p. 664.
[37] P.A. Huhn, M. Dornheim, T. Klassen, R. Bormann, Journal of Alloys and Compounds 404–406 (2005) 499.
[38] S.T. Oh, J.S. Lee, T. Sekino, K. Niihara, Scripta Materialia 44 (8–9) (2001) 2117–2120.
[39] F.P. Bowden, D. Tabor, The Friction and Lubrication of Solids, Clarendon Press, Oxford, 1986, p. 374.
[40] S.M. Hsu, Tribology International 37 (7) (2004) 537–545.